



ELSEVIER

Computer Physics Communications 147 (2002) 516–521

Computer Physics
Communications

www.elsevier.com/locate/cpc

A lattice Boltzmann study of reactive microflows

A. Gabrielli^a, S. Succi^{b,*}, E. Kaxiras^c

^a *INFN, Dipartimento di Fisica, Università di Roma “La Sapienza”, P. le A. Moro 2, 00185 Roma, Italy*

^b *CNR, Istituto di Applicazioni Calcolo, viale Policlinico 137, 00161 Roma, Italy*

^c *Lyman Laboratory of Physics, Harvard University, Cambridge, MA, USA*

Abstract

The role of geometrical micro-barriers for the conversion efficiency of reactive flows in narrow three-dimensional channels of millimetric size is investigated. Using a lattice Boltzmann–Lax–Wendroff code, we show that micro-barriers have an appreciable effect on the effective reaction efficiency of the device. If extrapolated to macroscopic scales, these effects can result in a sizeable increase of the overall reaction efficiency. © 2002 Published by Elsevier Science B.V.

PACS: 47.70.Fw; 47.11.+j

Keywords: Lattice Boltzmann; Heterogeneous catalysis; Micro-barriers

1. Introduction

One of the outstanding frontiers of modern applied physics/mathematics consists in the formulation of models and numerical tools for the description of complex phenomena involving multiple scales in space and time [1]. An important example of complex multiscale phenomena is the dynamics of reactive flows, a subject of wide interdisciplinary concern in theoretical and applied science. The complexity of reactive flow dynamics is parametrized by three dimensionless quantities: the *Reynolds number* $Re = UL/\nu$, the *Damkohler number* $Da = \tau_h/\tau_c$, and the *Péclet number* $Pe = UH/D$. Here U , L and H denote the macroscopic flow speed and longitudinal/transversal lengths of the flow, respectively, ν is the fluid kinematic viscosity and D the pollutant molecular diffusivity. The quantities τ_c and τ_h represent typical timescales of chemical and hydrodynamic phenomena. High Reynolds numbers are associated with turbulence. High Damkohler numbers imply that chemistry is much faster than hydrodynamics, so that reactions are always in chemical equilibrium and take place in tiny regions. In the opposite regime the chemistry is slow and always takes place at local mechanical equilibrium. Finally, high Péclet numbers imply that the transported species stick tightly to the fluid carrier. Varying *Re–Da–Pe* and considering different device morphologies meets with an enormous variety of chemico-physical behaviours [2]. In this work we deal with *low-Reynolds, fast-reacting flows with heterogeneous catalysis*. In particular we wish to gain insights into the role of geometric micro-irregularities for the effective absorption rate of tracer species at catalytic boundaries. For a detailed study see also [3].

* Corresponding author.

E-mail addresses: andrea@pil.phys.uniroma1.it (A. Gabrielli), succi@iac.rm.cnr.it (S. Succi).

2. Mathematical model of reactive microflow dynamics

We deal with a *quasi-incompressible, isothermal flow* with soluted species transported (advect and diffuse) by the flow and, upon reaching solid walls, undergoing *catalytic chemical reactions*. The basic equations of fluid motion are:

- (i) $\partial_t \rho + \operatorname{div} \rho \mathbf{u} = 0$ and
- (ii) $\partial_t \rho \mathbf{u} + \operatorname{div} \rho \mathbf{u} \mathbf{u} = -\nabla P + \operatorname{div}[2\mu(\nabla \mathbf{u} + (\nabla \mathbf{u})^T) + \lambda \operatorname{div} \mathbf{u}]$,

where ρ is the flow density, \mathbf{u} the flow speed, $P = \rho T$ the fluid pressure, T the temperature and μ, λ are the shear and bulk dynamic viscosities, respectively (for the present case of quasi-incompressible flow with $\operatorname{div} \mathbf{u} \simeq 0$ the latter can safely be ignored). Finally, $\mathbf{u} \mathbf{u}$ denotes the dyadic tensor $u_a u_b$, $a, b = x, y, z$.

Multispecies transport with chemical reactions is described by a generalized continuity-diffusion equation for each of $s = 1, \dots, N_s$ species:

$$\partial_t C_s + \operatorname{div} C_s \mathbf{u} = \operatorname{div}[D_s C_T \nabla(C_s/C_T)] + \dot{\Omega}_s \delta(\mathbf{x} - \mathbf{x}_w), \quad (1)$$

where C_s denotes the mass density of the generic s th species, D_s its mass diffusivity, $C_T = \sum_s C_s$ the total mass of transported species and $\dot{\Omega}_s$ is a chemical reaction term whose contribution is non-zero along the reactive surface described by the coordinate \mathbf{x}_w ($\delta(x)$ is the usual Dirac delta function). In the following the subscripts w and g mean “wall” (solid) and “gas” in a contact with the wall, respectively.

According to Fick’s law, the outgoing (bulk-to-wall) diffusive mass flux (molecules per unit surface and time) is given by (hereafter species index s is omitted for simplicity):

$$J_{g \rightarrow w} = -D \partial_{\perp} C_g |_{\text{wall}},$$

where ∂_{\perp} denotes the normal-to-wall component of the gradient. Upon contact with solid walls, the transported species react according to the following empirical rate equation:

$$\dot{\Omega} \equiv \frac{dC_w}{dt} = J_{g \rightarrow w} \frac{\Delta S}{\Delta V} - K_c C_w, \quad (2)$$

where ΔV is the volume element of the reactive wall and ΔS is the surface element across which fluid-wall mass transfer takes place. In our case the ratio

$\Delta V/\Delta S$ is simply the thickness of the reactive wall. K_c is the chemical reaction rate dictating species consumption once a molecule is absorbed by the wall. In the following we will use the common linear assumption

$$J_{g \rightarrow w} \frac{\Delta S}{\Delta V} = K_w (C_g - C_w), \quad (3)$$

where K_w is the wall-fluid mass transfer rate. In practice each boundary cell can be regarded as a microscopic chemical reactor sustained by the mass inflow from the fluid. Chemistry (Eqs. (2), (3)) sets a timescale for the steady-state mass exchange rate. At steady state we obtain:

$$C_w = \frac{K_w}{K_w + K_c} C_g.$$

Hence

$$J_{g \rightarrow w} \frac{\Delta S}{\Delta V} = \frac{C_g}{\tau_w + \tau_c},$$

where $\tau_w = 1/K_w$ and $\tau_c = 1/K_c$. These expressions show that finite-rate chemistry ($K_c > 0$) ensures a non-zero steady wall outflux of pollutant.

3. The computational method

The flow field is solved by a Lattice Boltzmann Equation (LBE) method [4–7] while the multispecies transport and chemical reactions are handled with a variant of the Lax–Wendroff method (LW) [8]. The LW scheme represents a numerically convenient choice recently developed to address multicomponent fluid transport (and reaction) within an LBE-like language.

3.1. Multiscale considerations

In this study, the unperturbed geometry of the catalytic device is a straight channel of size L lattice units along the flow direction (positive x -direction) and $H \times H$ across it (y - and z -axes). We add to this unperturbed geometry a single protrusion (barrier) of unitary thickness at a fixed $x = L/2$ with height h in the z -direction, and spanning the channel in the y -direction (see Fig. 1).

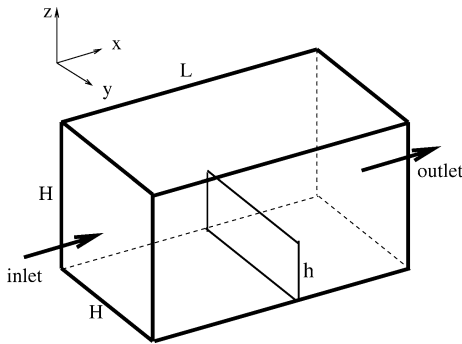


Fig. 1. Typical geometrical set-up of the channel flow with a barrier on the bottom wall perpendicular to the flow of height h .

This problem involves at least four relevant timescales. The relevant fluid scales are the advective and momentum-diffusive time:

$$\tau_A = L/U \quad \text{and} \quad \tau_v = H^2/\nu.$$

The relevant timescales for species dynamics are:

$$\tau_D = H^2/D, \quad \tau_w = K_w^{-1}, \quad \tau_c = K_c^{-1}.$$

As discussed in the introduction, they define the major dimensionless parameters

$$\begin{aligned} Re &= UH/\nu \equiv \tau_A/\tau_v, \\ Pe &= UH/D \equiv \tau_A/\tau_D, \\ Da_c &= \tau_c/\tau_A, \quad Da_w = \tau_w/\tau_A. \end{aligned} \quad (4)$$

4. Catalytic efficiency

The device efficiency is defined as the amount of pollutant burned per unit mass injected:

$$\eta = \frac{\Phi_{\text{in}} - \Phi_{\text{out}}}{\Phi_{\text{in}}}, \quad (5)$$

where $\Phi(x) = \int [uC](x, y, z) dy dz$ is the longitudinal mass flow of the pollutant at section x and u is the x component of \mathbf{u} (v and w will be the y and z components, respectively). The in–out longitudinal flow deficit is equal to the amount Γ of pollutant absorbed at the catalytic wall per unit time.

The goal of the optimization problem is to maximize Γ at a given Φ_{in} . This means maximizing complex configuration-dependent quantities, such as the wall distribution of the pollutant and its normal-to-wall gradient. For future purposes, we find it convenient to recast the catalytic efficiency as $\eta = 1 - T$,

where T is the channel *transmittance* $T \equiv \Phi_{\text{out}}/\Phi_{\text{in}}$. Roughly speaking, in the limit of fast chemistry, this is controlled by the ratio of advection to diffusion timescales. It is intuitive that high efficiencies are associated with large values of the ratio τ_A/τ_D , namely low Péclet numbers.

5. The role of micro-irregularities

We now discuss the main qualitative effect of the micro-barrier from a microscopic point of view.

Firstly, it provides a potential enhancement of reactivity via the increase of the surface/volume ratio. How much of this potential is actually realized depends on the resulting flow configuration.

Here, the fluid plays a two-faced role. First, geometrical restrictions lead to local fluid acceleration, hence less time for the pollutant to migrate from the bulk to the wall before being convected away by the mainstream flow. This effect may become appreciable on micro-scales for micro-flows with $h/H \simeq 0.1$ (as in actual catalytic converters). Moreover, obstacles shield away part of the active surface (wake of the obstacle) where the fluid circulates at much reduced rates (stagnation) so that less pollutant is fed into the active surface. The size of the shielded region is proportional to the Reynolds number of the flow. On the other hand, if by some mechanism the flow proves capable of feeding the shielded region, then efficient absorption is restored simply because the pollutant is confined by recirculating patterns and has almost infinite time to react without being convected away. This case is met mainly in the presence of sufficiently energetic turbulent fluctuations at high values of the *micro-barrier* Péclet number $Pe_h = w'h/D \gg 1$ where w' is the z -component of the velocity field at the barrier tip.

With some appropriate approximations [3], one can show that the efficiency is:

$$\eta_0 \simeq 1 - e^{-L/l}, \quad (6)$$

where $l = l_{\perp}^2 \bar{U}/D$, $\bar{U} = \sum_{y,z} uC / \sum_{y,z} C$, $l_{\perp}^2 = C\tau H^2/(2C_g)$ and $\tau \simeq (1/\tau_D + 1/(\tau_c + \tau_w))^{-1}$.

Note that in the low absorption limit $L \ll l$, the above relation is reduced to $\eta_0 \simeq L/l$, meaning that halving, say, the absorption length implies the same efficiency with a twice shorter catalyzer. In the

opposite high-absorption limit, $L \gg l$, the relative pay-off becomes increasingly less significant.

We now turn to the case of a “perturbed” geometry. Let us begin by considering a single barrier of height h (Fig. 1). The reference situation is a smooth channel at high Damkohler (Eq. (6)).

From [3] we find an estimate of perturbative corrections in the smallness parameter $g \equiv h/H$:

$$\frac{\delta\eta}{\eta_0} \simeq \frac{A}{2} \frac{h}{H} Re_h [Sc + K(a - 1)], \quad (7)$$

where $A = H/L$ is the aspect ratio of the channel, $Sc = \nu/D$ is the Schmidt number, and a is a regime-dependent parameter. The wake length W can be estimated by $W/h = KRe_h$ with $K \simeq 0.1$. Three distinctive cases can be identified:

- (i) $a = 0$: the wake region is totally deactivated, absorption zero;
- (ii) $a = 1$: absorption in the wake region is exactly the same as for unperturbed flow;
- (iii) $a > 1$: the wake absorption is higher than with unperturbed flow (back-flowing micro-vortices can hit the rear side of the barrier).

6. Application: reactive flow over a micro-barrier

The computational scheme has been applied to a fluid flowing in a millimeter-sized box of size $2 \times 1 \times 1$ millimeters along the x, y, z directions with a perpendicular barrier of height h (see Fig. 1). Upon using a $80 \times 40 \times 40$ grid, we obtain a lattice with $dx = dy = dz = 0.0025$ ($25 \mu\text{m}$). We assume a real sound speed $V_s = 300$ m/s which becomes $c_s = 1/\sqrt{3}$ in lattice units. Therefore a time step is equivalent to $dt = c_s dx/V_s \simeq 50$ ns.

The flow is forced with a constant volumetric force which mimics the effects of a pressure gradient. The fluid flow carries a passive pollutant which is continuously injected at the inlet with a flat profile across the channel. Diffusing across the flow, it reaches solid walls where it reacts according to a first-order catalytic reaction: $C + A \rightarrow P$, where A denotes an active catalyzer and P the reaction products. The initial conditions are:

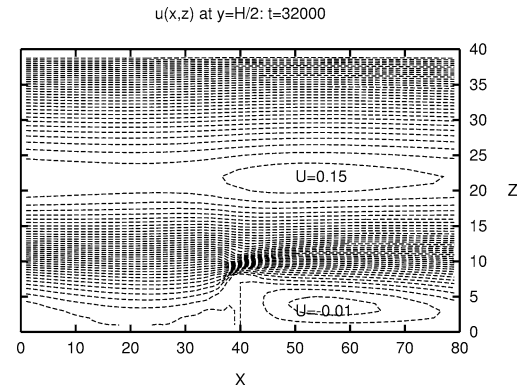


Fig. 2. Typical two-dimensional cut of the flow pattern with a single barrier of height $h = 8$. Streamwise flow speed in the plane $y = H/2$.

$$C(x, y, z) = \begin{cases} 1 & \text{at the inlet,} \\ 0 & \text{elsewhere,} \end{cases}$$

$$\rho(x, y, z) = 1,$$

$$u(x, y, z) = U_0,$$

$$v(x, y, z) = w(x, y, z) = 0.$$

The pollutant is then released at the open outlet, while flow periodicity is imposed at the inlet/outlet boundaries. On the upper and lower walls, the flow speed is forced to vanish, whereas the fluid-wall mass exchange is modeled via a mass transfer rate equation of the form previously discussed. Our simulations refer to the following values (in lattice units): $U_0 \simeq 0.1-0.2$, $D = 0.1$, $\nu = 0.01$, $K_c = K_w = 0.1$. This implies $Pe \simeq 40$, $Re \simeq 400$, $Da > 80$ (see also Eq. (4)). In order to study the effects of the barrier height h , we consider the following values: $h = 0, 2, 4, 8$. The typical simulation time is $t = 32,000$ time steps (about 1.6 milliseconds in physical time) corresponding to two mass diffusion times across the channel. We may estimate the reference efficiency for the case of a smooth channel: with $\bar{U} \simeq 0.1$, and $\tau = 20$, we obtain $l \simeq 200$, hence $\eta_0 \simeq 0.33$.

A typical two-dimensional cut of the flow pattern and pollutant spatial distribution in the section $y = H/2$ is shown in Figs. 2 and 3, which refer to the case $h = 8$. An extended (if feeble) recirculation pattern is well visible past the barrier. Also, enhanced concentration gradients on the tip of the barrier are easily recognized from Fig. 3. The integrated concentration of the pollutant $C(x) = \sum_{y,z} C(x, y, z)$ is presented in Fig. 4 for the cases $h = 0, 2, 4, 8$. The main highlight

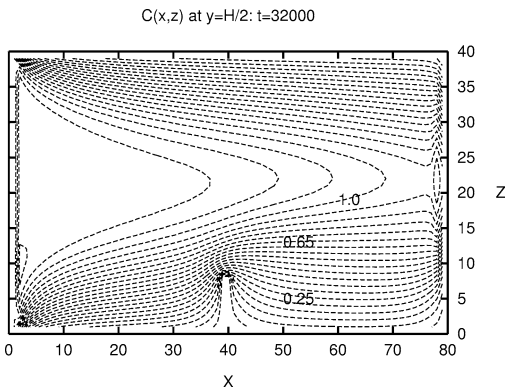


Fig. 3. Concentration isocontours with a single barrier of height $h = 8$ on the plane $y = H/2$.

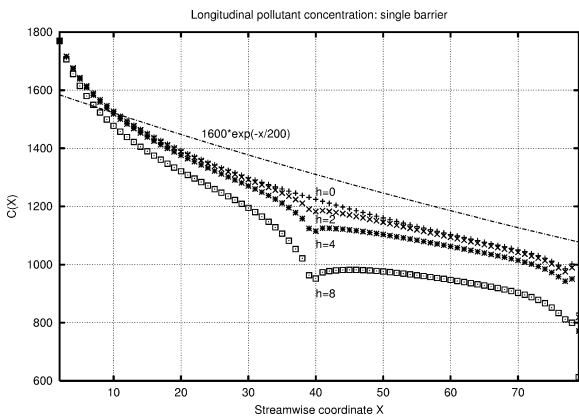


Fig. 4. Integrated concentration $C(x)$ of the pollutant with a single barrier of height $h = 0, 2, 4, 8$ after 32,000 steps. The dashed line represent a theoretical evaluation with no barrier ($h = 0$) and $l \approx 200$.

is a substantial reduction of the pollutant concentration with increasing barrier height. We measure also the pollutant longitudinal mass flow $\Phi(x)$. The efficiency η is defined by Eq. (5). The results are shown in Table 1, where subscript A refers to Eq. (7) with $a = 1$. These results are in reasonable agreement with the analytical estimate apart from deviations at $h = 8$ for which the overall efficiency is overestimated. Leaving aside the initial portion of the channel, our numerical data are pretty well fitted by an exponential with absorption length $l = 200$, in good agreement with the theoretical estimate $l \approx 200$. The barrier also promotes a potentially beneficial flow recirculation, which is well visible in Figs. 5 and 6. They clearly reveal a

Table 1
Single barrier at $x = 40$: the effect of barrier height

Run	h/H	η	$\delta\eta/\eta, \delta\eta_A/\eta_A$
R00	0	0.295	0.00
R02	1/20	0.301	0.02, 0.025
R04	1/10	0.312	0.06, 0.10
R08	2/10	0.360	0.22, 0.40

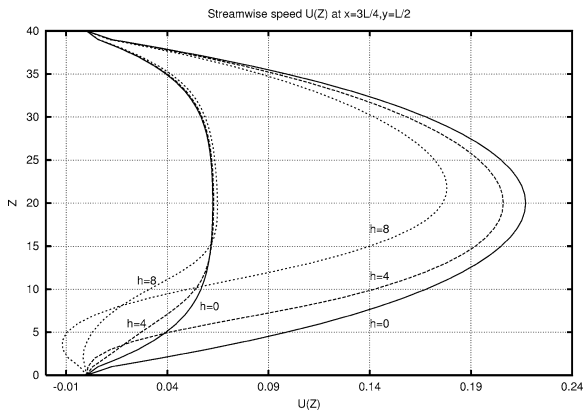


Fig. 5. Time evolution of the transversal streamwise speed $u(z)$ at $x = 3L/4$ and $y = L/2$. Single barrier of varying height $h = 0, 4, 8$ at $t = 3200$ and $t = 32,000$. Note the backflow for $h = 8$ at small z .

Stream function at $y=L/2$: $h=8$, 160000 time steps

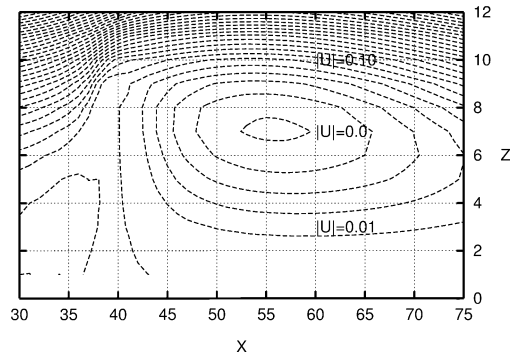


Fig. 6. Blow-up of the streamlines of the flow field past a barrier of height $h = 8$ located at $x = 40$. The velocity direction in the closed streamlines of the vortex is clockwise. The recirculation effects are feeble and depletion is dominant. In fact for $h = 8$ the local Reynolds number is $\sim 0.01 \cdot 8/0.01 = 8$, seemingly too small to provide micro-turbulent effects.

recirculating backflow for $h = 8$. For applications to many barriers see [3].

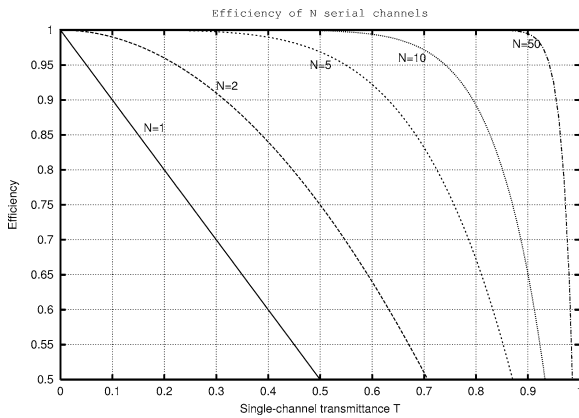


Fig. 7. Efficiency of a series of N micro-channels as a function of the single-channel transmittance.

7. Upscaling to macroscopic devices

It is important to realize that even tiny improvements on the microscopic scale can result in pretty sizeable cumulative effects on the macroscopic scale of the real devices, say 10 centimeters. The efficiency of an array of N serial micro-channels can be estimated simply as

$$\eta_N = 1 - T^N. \quad (8)$$

It is readily recognized that even low single-channel efficiencies can result in significant efficiencies of macroscopic devices with $N = 10$ – 100 (see Fig. 7). Eq. (8) with numerical data from present simulations provide satisfactory agreement with experimental data [9,10].

Nonetheless, extrapolations based on Eq. (8) must be taken very cautiously in the case of rough or fractal walls [11] or of fully developed turbulence.

8. Conclusions

Although these simulations generally confirm qualitative expectations on the overall dependence on the major physical parameters, they also highlight the existence of non-perturbative effects, such as the onset of micro-vorticity in the wake of geometrical obtrusions, which are hardly amenable to analytical treatment.

Acknowledgement

Sauro Succi thanks the Physics Department of Harvard University for his Visiting Scholar appointment and for its hospitality during his stay. Work performed under NATO Grant PST.CLG. 976357.

References

- [1] F. Abraham, J. Broughton, N. Bernstein, E. Kaxiras, *Comp. in Phys.* 12 (1998) 538.
- [2] E. Oran, J. Boris, *Numerical Simulation of Reactive Flows*, Elsevier Science, New York, 1987.
- [3] S. Succi, A. Gabrielli, G. Smith, E. Kaxiras, *European Phys. J. Appl. Phys.* 16 (2001) 71.
- [4] G. McNamara, G. Zanetti, *Phys. Rev. Lett.* 61 (1988) 2332.
- [5] F. Higuera, S. Succi, R. Benzi, *Europhys. Lett.* 9 (1989) 345.
- [6] R. Benzi, S. Succi, M. Vergassola, *Phys. Rep.* 222 (1992) 145.
- [7] Y. Qian, D. d'Humieres, P. Lallemand, *Europhys. Lett.* 17 (1989) 149.
- [8] S. Succi, G. Bella, H. Chen, K. Molvig, C. Teixeira, *J. Comp. Phys.* 152 (1999) 493.
- [9] S. Succi, G. Smith, E. Kaxiras, *J. Stat. Phys.* 107 (1–2) (2002) 343.
- [10] A. Bergmann, R. Bruck, C. Kruse, Society of Automotive Engineers (SAE) technical paper SAE 971027, in: *Proceedings of the 1997 International SAE Congress*, Detroit, USA, February 1997.
- [11] J.S. Andrade Jr, M. Filoche, B. Sapoval, *Europhys. Lett.*, to appear, cond-mat/0012258; <http://xxx.lanl.gov>.